J Neurophysiol 90: 1921–1935, 2003.
First published May 7, 2003; 10.1152/jn.00623.2002.

Dendrodendritic Inhibition and Simulated Odor Responses in a Detailed Olfactory Bulb Network Model

Andrew P. Davison, Jianfeng Feng, and David Brown
Neurobiology Programme, The Babraham Institute, Babraham, Cambridge CB2 4AT, United Kingdom

Submitted 1 August 2002; accepted in final form 24 April 2003

Davison, Andrew P., Jianfeng Feng, and David Brown. Dendrodendritic inhibition and simulated odor responses in a detailed olfactory bulb network model. *J Neurophysiol* 90: 1921–1935, 2003. First published May 7, 2003; 10.1152/jn.00623.2002. In the olfactory bulb, both the spatial distribution and the temporal structure of neuronal activity appear to be important for processing odor information, but it is currently impossible to measure both of these simultaneously with high resolution and in all layers of the bulb. We have developed a biologically realistic model of the mammalian olfactory bulb, incorporating the mitral and granule cells and the dendrodendritic synapses between them, which allows us to observe the network behavior in detail. The cell models were based on previously published work. The attributes of the synapses were obtained from the literature. The pattern of synaptic connections was based on the limited experimental data in the literature on the statistics of connections between neurons in the bulb. The results of simulation experiments with electrical stimulation agree closely in most details with published experimental data. This gives confidence that the model is capturing features of network interactions in the real olfactory bulb. The model predicts that the time course of dendrodendritic inhibition is dependent on the network connectivity as well as on the intrinsic parameters of the synapses. In response to simulated odor stimulation, strongly activated mitral cells tend to suppress neighboring cells, the mitral cells readily synchronize their firing, and increasing the stimulus intensity increases the degree of synchronization. Preliminary experiments suggest that slow temporal changes in the degree of synchronization are more useful in distinguishing between very similar odorants than is the spatial distribution of mean firing rate.

INTRODUCTION

The main olfactory bulb receives signals from the population of olfactory receptor neurons and transmits signals to the olfactory cortex, the limbic system, and other brain regions. Mapping of the sensory inputs has revealed that each odorant produces a reproducible spatial pattern of activation in the glomerular layer of the bulb (reviewed in Xu et al. 2000). This pattern is transformed in the bulb by lateral interactions between mitral and tufted (M/T) cells. The secondary dendrites of M/T cells extend long distances, allowing the M/T cells innervating one glomerulus to communicate, via interneurons, with M/T cells dispersed widely across the bulb. Evidently the spatial patterning of both inputs and interactions is important in olfactory bulb information processing (Luo and Katz 2001). The spatial pattern alone may not be sufficient, however; there is evidence that the temporal patterning of bulbar activity has functional relevance. The evidence for the role of fine- and coarse-scale temporal patterns in the antennal lobe (the insect analogue of the olfactory bulb) is reviewed in Laurent et al. (2001). Global oscillations (Adrian 1942) and synchronization between mitral cells (Kashiwadani et al. 1999; Schoppa and Westbrook 2001) have been seen in the mammalian olfactory bulb.

Most studies of odor coding in the olfactory bulb/antennal lobe have, of necessity, focused on either the spatial or the temporal aspects. Electrophysiological recordings have excellent time resolution but can follow only a few individual neurons, or the averaged activity of many. Imaging methods can record the activity of neurons across half the bulb, but with spatial resolution on the order of the size of a glomerulus, not a single neuron, and with temporal resolution on the order of hundreds of milliseconds, not single action potentials. In contrast, detailed, biologically realistic, quantitative modeling can potentially simulate every neuron in the olfactory bulb with submillisecond temporal resolution and can integrate the results from the different experimental modalities.

We have developed a biologically realistic model of a mammalian olfactory bulb. Our main hypothesis is that lateral inhibition and network synchronization will arise naturally from a model consisting only of mitral and granule cells, with parameters obtained from the literature and not from tuning the model. The model was tested by performing simulation experiments studying dendrodendritic synaptic currents and comparing the results to published experimental data (Schoppa et al. 1998). There was good agreement between model and data, which gives confidence that the model is capturing features of network interactions in the real olfactory bulb. We then investigated the model's response to odor stimulation. We found that strongly activated mitral cells tend to suppress neighboring cells, that the mitral cells readily synchronize their firing, and that increasing the stimulus intensity increases the degree of synchronization. Synchronization is reduced by high-frequency modulation (FM) of the input intensity such as might be found during active sniffing. Preliminary experiments suggest that slow temporal changes in the degree of synchronization are more useful than the spatial activity map in distinguishing between very similar odorants.

The model predicts that *1*) increasing the number of activated synapses onto granule cells will lengthen the duration of

Address for reprint requests: A. P. Davison, Unité de Neurosciences Intégratives et Computationelles, Institut de Neurobiologie Alfred Fessard, Centre Nationale de la Recherche Scientifique, 1 Avenue de la Terrasse, 91198 Gif sur Yvette, France (E-mail: andrewdavison@fastmail.fm).

The costs of publication of this article were defrayed in part by the payment of page charges. The article must therefore be hereby marked "*advertisement*" in accordance with 18 U.S.C. Section 1734 solely to indicate this fact.

lateral inhibition in mitral cells; and *2*) increasing the odor intensity will increase the degree of synchronization. Experimental testing of these and other predictions is now required.

METHODS

In this section, we describe the model, with an emphasis on the approximations and simplifications that were made. The model is available from the SenseLab ModelDB database at http://senselab.med.yale.edu.

Cell types

The major neuron types that have been described in the olfactory bulb are mitral cells, tufted cells, periglomerular (PG) cells, granule cells, and short-axon cells. The decision as to which of these cell types should be included in a model is based primarily on the contribution each is thought to make to the network behaviors of interest (i.e., a cell type which makes a large contribution must be included, while one which makes a minor contribution may be excluded) and secondarily on the information that is available about each cell type (i.e., little is gained by including a poorly characterized cell type in the model). In summary, there must be a trade-off between completeness and simplicity.

The mitral/tufted cells and the granule cells are thought to form the fundamental circuit of the olfactory bulb. Detailed models of these cell types have been published (Bhalla and Bower 1993), and in previous work we have simplified these detailed models so they are fast enough to be used in large networks (Davison 2001; Davison et al. 2000). Therefore these cell types have been included in the model.

The short-axon cells are present in small numbers compared with the other cell types, which suggests that their role in the processing carried out by the bulb may be small, and almost nothing is known about their physiology; therefore we have not included these cells in the model.

The decision whether or not to include periglomerular neurons is difficult. The population of periglomerular cells is large and their synaptic connections are fairly well understood. Less is known about the physiology of these cells than about mitral and granule cells, although there have been measurements of sodium and potassium channel kinetics in frogs (Bardoni et al. 1995, 1996) and in rats (Puopolo and Belluzzi 1996, 1998), and PG cell responses to current injection have been characterized (McQuiston and Katz 2001). Detailed reconstructions of the cell morphology for compartmental modeling have not been made. In evolutionary terms, periglomerular cells appeared late—they are not present at all in fish and are most numerous in mammals (Dryer and Graziadei 1994). This suggests that PG cells provide a refinement of the bulb's fundamental computations supposed to be performed by the mitral/tufted-granule cell system. On balance, we have decided not to include PG cells in this model, although future extensions of the model could include these cells.

Is it necessary to model mitral and tufted cells separately? Both types are output neurons and have similar morphology—glomerular tuft and extensive lateral dendrites—but there are also many differences between them: in size, in orthodromic response properties (Ezeh et al. 1993; Schneider and Scott 1983), in axonal projection patterns to central olfactory areas, in the distribution of secondary dendrites (Mori et al. 1983; Orona et al. 1984), and of local axon collaterals (Kishi et al. 1984). The differences in the distribution of secondary dendrites, together with the different dendritic branching patterns of granule cell subtypes, mean that there is less communication between the mitral and tufted cell populations than within them. Adding to this the differences in axonal projection patterns leads to the idea of a functional separation between the mitral and tufted cell populations (Mori et al. 1983). We conclude that tufted cells need not be modeled explicitly to gain basic insights into olfactory bulb function, although they must be included as the model is developed and we gain a fuller picture.

The mitral cell and granule cell models are morphologically simplified versions of the detailed compartmental models published by Bhalla and Bower (1993). The simplified models run about 60 times faster than the original detailed models but closely reproduce the firing patterns of the detailed models. The simplified mitral cell model has four compartments, representing soma/axon, secondary dendrites, primary dendrite shaft, and primary dendrite tuft. The simplified granule cell model has three compartments, representing soma, deep dendrites, and peripheral dendrite. Full details of the simplified models are given in Davison et al. (2000) (mitral cell) and in Davison (2001) (mitral and granule cells).

Network connectivity

As the olfactory bulb is laminar, it is convenient to describe it by a two-dimensional network, with the direction perpendicular to the laminae not explicitly represented. To represent the shape of the bulb, the network topology should be defined by the surface of some ellipsoid. A planar network, however, makes calculation of location and distance much easier. The arrangement of mitral and granule cells, and the connections between them, are shown in Fig. 1. Both mitral and granule cells are arranged in square arrays. The separation between granule cells is taken as unity, and both the separation between mitral cells and the length of mitral cell secondary dendrites are expressed as a multiple of this unit granule cell separation. The mitral cells were either all grouped into a single glomerulus, in which case the mitral cell separation was taken as zero, for computational simplicity, or each mitral cell represented a different glomerulus, in which case the mitral cell separation was the square root of the ratio of the number of granule cells to mitral cells.

The numbers of mitral and granule cells in rodent olfactory bulb are in the region of 5×10^4 and 5×10^6, respectively (Hinds and McNelly 1977; Panhuber et al. 1985; Royet et al. 1998; Shepherd and Greer 1998). Lacking the computational resources to simulate so many cells, the size of the network must be reduced. This may be done either by reducing the extent of the network (which ignores inputs from cells outside the network; these may be significant, given the long length of mitral cell secondary dendrites) or by making the network more sparse (which changes either the number of connections per cell or the degree of connectivity between cells). We have used both strategies. Modeling a single glomerulus reduces the number of cells by a factor of about 1,000 and if only that glomerulus is stimulated the problem of outside inputs is removed (except for background activity). To model multiple glomeruli, we have used only one mitral cell per glomerulus and attempt to infer the behavior of the full network from the behavior of the smaller one. This simplification may be reasonable since there is evidence that mitral

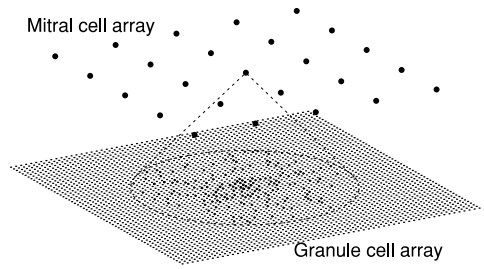

FIG. 1. Mitral–granule cell network. Mitral cells are shown as large dots. Each mitral cell makes n_{syn} connections to granule cells selected randomly from all the cells within its "arbor" (shown as a circle). $n_{syn} = 200$. Granule cells connected to the central mitral cell are shown as intermediate-size dots. There are fewer connected cells than connections since some granule cells have more than 1 connection to the mitral cell. Remaining granule cells are shown as the smallest dots.

cells innervating the same glomerulus tend to have synchronized firing (Schoppa and Westbrook 2001). We have simulated between 25 and 100 mitral cells and between 144 and 14,400 granule cells. The numbers used for each simulation experiment are given in the relevant section of RESULTS.

A simple method of specifying which mitral cells are connected to which granule cells was adopted. We make the simplifying assumption that the probability of a mitral cell forming a synapse at a point depends only on the radial distance from the soma and not on the direction. This is an approximation, since dendrites project in definite directions from the soma, but the dendrites branch copiously, so the approximation appears reasonable. The probability of forming a synapse is zero outside a certain radius determined by the length of the mitral cell secondary dendrites. In the model this radius was set, except where noted otherwise, to one-half the extent of the granule cell array so as to maximize the number of granule cells inside the mitral cell dendritic arbor. The trade-off for this is that we are then modeling only a limited region of the bulb. Inside this radius, for each mitral cell synapse, a direction and distance were each chosen at random from uniform distributions, defining a point in the plane. A connection was then made with the granule cell whose location was nearest to this point.

The number of synapses can be estimated to be on the order of 10^4 per mitral cell (see Davison 2001 for more details). Due to limitations of computer resources, however, only a few hundred synapses per mitral cell could be included in the model.

In some simulations we added GABA synapses between granule cells. The existence of inhibitory synapses onto the deep or basal dendrites of granule cells was shown by Price and Powell (1970). Wellis and Kauer (1994) further demonstrated that granule cells receive hyperpolarizing GABAergic input. Finally, Nusser et al. (2001) demonstrated that disruption of $GABA_A$ receptors on granule cells affects network activity.

Based on published camera lucida drawings (cat, Mori et al. 1983; rat, Orona et al. 1983), the maximum extent of granule cell basal dendrites is 50–100 μm. This compares to 850 μm for the radius of the mitral cell secondary dendritic field (rabbit, Mori et al. 1983). Based on this evidence we set the radius of granule–granule connections to be 1/10 the radius of mitral–granule connections. The mean number of spines on granule cell basal dendrites ranges from 26 to 42 depending on subtype (Mori et al. 1983). Assuming one synapse per spine and further assuming that all synapses onto these basal spines are from granule cells (there may also be centrifugal connections from outside the bulb), the cells in the model receive and make 40 granule–granule cell connections. Note that action potentials do not propagate into the basal dendrites of the granule cell model, so for convenience the granule–granule cell synapses were triggered by an action potential measured in the peripheral dendrite.

We did not include synapses onto granule cells from mitral cell axon collaterals, as the influence of such connections on mitral–granule cell interactions is secondary to that of the dendrodendritic synapses (Shepherd and Greer 1998). We have not attempted to model gap junctions between granule cells (Reyher et al. 1991) because of the lack of information on the functional consequences of such junctions. Finally, we have not modeled any of the self- and mutually excitatory interactions between mitral cells hypothesized to arise from extrasynaptic glutamate diffusion (Didier et al. 2001; Isaacson 1999; Schoppa and Westbrook 2001). These interactions are much smaller than, and are masked by, the dendrodendritic inhibitory synaptic currents. As secondary effects, they were therefore excluded from the current model to retain simplicity.

Synapses

The mitral cell secondary dendrite and granule cell peripheral dendrite compartments were reciprocally connected by spike-triggered synapses. The granule–mitral synapse has $GABA_A$ receptors, the mitral–granule synapse has both AMPA and *N*-methyl-D-aspartate (NMDA) receptors. For the AMPA and $GABA_A$ synapses, the synaptic response was modeled as an instantaneous step in conductance followed by exponential decay. For the NMDA receptor, the conductance has a finite rise time, followed by exponential decay. There is a time delay between the presynaptic spike and the onset of the postsynaptic response. The expressions for the synaptic currents are given in the APPENDIX. Values of the maximal conductances and synaptic time constants were obtained from the literature and are as follows. Except where noted, all values are from Schoppa et al. (1998). Unitary inhibitory postsynaptic currents (IPSCs) recorded in mitral cells have a peak amplitude of about 40 pA and decay time constant of 18 $\pm$ 1 ms, with the chloride reversal potential maintained near 0 mV and the holding potential at -70 mV. This gives a maximal conductance of 0.6 nS per synapse. The rise time is about 4 ms, but for simplicity, an instantaneous rise was modeled. The decay time constant of the fast component of the excitatory postsynaptic current (EPSC) in granule cells has been measured as 5.5 $\pm$ 1.2 ms. The rise time of the NMDA current is about 30 ms. The rise time constant has not been measured experimentally so we used a value of 52 ms based on estimation. The decay phase has been fitted with two components with time constants 52 $\pm$ 10 and 343 $\pm$ 48 ms. The relative amplitudes of these components were not specified. For simplicity, therefore, we have used a single exponential decay with time constant 343 ms. The peak of the fast (AMPA) component of the EPSC recorded in granule cells is approximately 60 pA (Isaacson and Strowbridge 1998; Schoppa et al. 1998). Assuming a difference of about 60 mV between holding and reversal potentials gives a maximal conductance of 1.0 nS per synapse. The peak amplitude of the NMDA current is 0.26 $\pm$ 0.05 times that of the AMPA current in magnesium-free conditions, giving a peak conductance of 0.26 nS, but due to the nonzero rise time, this is not the same as the maximal conductance, which can be calculated to be 0.59 nS using *Eqs. 7* and *8* in the APPENDIX.

Miniature IPSCs (mIPSCs) in granule cells have a time constant of 8.3 $\pm$ 0.6 ms (Nusser et al. 2001), shorter than in mitral cells. The peak amplitude of the mIPSCs was 74.8 $\pm$ 11.9 pA with a holding potential of -70 mV and symmetrical chloride concentrations, giving a peak conductance of 1.1 nS. This is larger than in mitral cells, but due to the faster time constant, the total charge transfer is similar in both cell types.

The ideal way to determine the synaptic time delays is to record simultaneously from mitral and granule cells and measure the time between a mitral cell spike and the onset of the excitatory postsynaptic potential (EPSP) in the granule cell, and the time between a granule cell spike and the onset of the inhibitory postsynaptic potential (IPSP) in the mitral cell. To our knowledge, such a recording has not been carried out, so we must rely on more indirect data. Mori and Takagi (1978) measured the time between the arrival of an antidromic spike at the mitral cell soma (inferred from field potential recordings) and the onset of an EPSP in a granule cell (from intracellular recording), obtaining a value of 1.8 $\pm$ 0.3 ms. The time between the arrival of the antidromic spike and the onset of an IPSP in mitral cells was 2.4 $\pm$ 0.4 ms, giving a time delay for the granule–mitral synapse of at most 0.6 ms. In the absence of information about the time delay of granule–granule synapses, we used a value of 0.6 ms. The synaptic parameters are summarized in Table 1.

TABLE 1. *Synaptic parameters*

$\bar{g}_{AMPA}$	1.0 nS	$\bar{g}_{NMDA}$	0.593 nS
$\bar{g}_{GABA_A}$	0.6 nS	$\bar{g}^g_{GABA_A}$	1.1 nS
τ_{AMPA}	5.5 ms	τ_{GABA_A}	18 ms
τ^{α}_{NMDA}	52 ms	τ^{β}_{NMDA}	343 ms
$\tau^{g}_{GABA_A}$	8.3 ms	t_{dur}	30 ms
t^E_d	1.8 ms	t^I_d	0.6 ms
E_E	0 mV	E_I	-70 mV

An explanation of the terms is given in the APPENDIX.

Network inputs

The mitral cells were stimulated by current injection to the apical dendrite (glomerular) compartment. For focal electrical stimulation all cells received a short current pulse of fixed amplitude. For odor inputs each cell received a different level of input (current amplitude). Only a few cells received strong currents; most received weak currents. This was intended to mimic the findings of odor mapping studies that simple chemical odors strongly activate only a subset of all glomeruli (see Xu et al. 2000 for a review). The relative amplitudes of the inputs to the different cells were fixed for a particular "odor," but the absolute amplitude ("odor concentration") could be changed. In most of the simulations, the odor concentration (current amplitude) was not changed with time, to see the steady-state response of the network. In one set of simulations the odor concentration was varied sinusoidally. Using a continuous current for the input mimics a time-averaged olfactory receptor neuron response. This method has the advantages of simplicity and computational speed. The principal disadvantage is that it is less noisy than a synaptic stimulus arising from a real spike train.

Numerical methods

The model was simulated in NEURON (Hines and Carnevale 1997) (available from www.neuron.yale.edu). Both the backward Euler method with time step 25 μs and a multi-order locally variable time-step method with absolute tolerance of 0.01 were used to integrate the model. A few simulations were repeated with time step 0.1 μs or absolute tolerance of 10^{-6} to check that the larger time step/larger tolerance was adequate.

Synchronization index

Perfect or near-perfect synchrony can easily be recognized in the spike time raster plots of the cell population. Phase-locking and partial synchronization are much more difficult to discern. Therefore a numerical index is necessary to identify and quantify synchronization and phase-locking. We use an index that is sensitive to phase-locking (synchronization being the special case with zero phase difference), based on statistics of the phase-lag between spikes in different cells. The phase-lags are calculated as follows: for each mitral cell k ($k = 1, \ldots, n$) in the network, for each spike time t_i^k ($i = 2, \ldots N_{k-1}$) (where N_k is the number of spikes in cell k) of that cell except the first and last, we find the closest spike time t_j^l in every other cell l ($l = 1, \ldots, n$; $l \neq k$), provided that spike is within one-half the inter-spike interval. The time lag for spike time t_i^k with respect to cell l is then defined by $\ell_i^{kl} = t_j^l - t_i^k$. The phase lag ϕ_i^{kl} is defined by

$$\phi_i^{kl} = \begin{cases} \ell_i^{kl}/(t_i^k - t_{i-1}^k) & \ell_i^{kl} < 0 \\ \ell_i^{kl}/(t_{i+1}^k - t_i^k) & \ell_i^{kl} \geq 0 \end{cases} \quad (1)$$

The phase-locking index, σ, is defined by

$$\sigma = \left(\frac{1}{n(n-1)} \sum_{k=1}^{n} \sum_{\substack{l=1 \\ l \neq k}}^{n} \mathrm{Var}(\phi_i^{kl}) \right)^{1/2} \quad (2)$$

where $\mathrm{Var}(\phi_i^{kl})$ is the variance of the phase lags ϕ_i^{kl} of cell k with respect to cell l. The smaller the index, the better is the phase-locking. In the case of all spikes in all cells being perfectly phase-locked, $\sigma = 0$. We will also refer to σ as the synchronization index, since the phase lags are usually a small fraction of the inter-spike interval.

RESULTS

Response to focal electrical stimulation

The dendrodendritic reciprocal synapse has a central role in olfactory bulb function, and therefore it is desirable to test this aspect of the model with reference to experimental results. Schoppa et al. (1998) recorded synaptic currents in mitral and granule cells in response to focal electrical stimulation of one glomerulus, giving a detailed picture of dendrodendritic function. In this experiment, the bulb model was simulated with the same conditions, as far as possible, as used by Schoppa et al.

The somata of mitral cells innervating a single glomerulus are likely to be distributed within a small area (one study found that 96% of mitral cells connected to the same glomerulus were separated by <120 μm (Buonviso et al. 1991). For simplicity in determining connections, the model assumes that the somata are located at a single point, and therefore the range of connections can be set to the entire extent of the cell array.

The size of the mitral cell array was 5×5. To reduce synchronization of cell firing, some heterogeneity was added to the network by picking $\bar{g}_{\mathrm{NMDA}}$ for each cell from a normal distribution with SD equal to one-half the mean. This method of adding heterogeneity was chosen arbitrarily to obtain the desired effect. One mitral cell was voltage clamped at -70 mV with a series resistance of 2 MΩ and the chloride reversal potential set to 0 mV to measure synaptic currents in this cell. All mitral cells were stimulated simultaneously in the glomerular compartment with a current pulse of amplitude 20 nA and duration 5 ms. The extracellular magnesium concentration, $[Mg^{2+}]$, was set to 0 mM. The model was simulated for 3,000 ms.

The network model responds to short-duration glomerular stimulation with a single action potential in each mitral cell (Fig. 2*A*) and a train of action potentials in granule cells (e.g., Fig. 2*B*). The duration and frequency of this spike train depends on the number of synaptic inputs each granule cell receives. The granule cell population response is an initial, synchronized burst followed by unsynchronized firing (Fig. 2*D*) with an exponentially decaying spike-time histogram (STH; Fig. 2*E*). The prolonged granule-cell firing produces a long-duration IPSC in the voltage-clamped mitral cell. This IPSC was fitted between 50 and 1,500 ms with a single exponential function (time constant, 310 ms), although the sum of two exponentials (time constants 78 and 487 ms) gave a better fit. This IPSC is similar in amplitude and time-course to that seen experimentally by Schoppa et al. (1998; their Fig. 1*A*), except that the model time constant (310 ms) is shorter than the experimental time constant (540 ms).

Effect of Mg^{2+}

The previous simulation was carried out with $[Mg^{2+}] = 0$ mM. We investigated the effect of magnesium ion concentration on the model by simulating the mitral cell IPSC for different values of $[Mg^{2+}]$ (Fig. 3*A*). The effect of increasing $[Mg^{2+}]$ is to shorten the prolonged component of the IPSC, with little or no effect on the early component. The total charge transferred to the mitral cell may be found by integrating the IPSC curve over time. Figure 3*B* shows the total charge (as a fraction of the total charge at $[Mg^{2+}] = 0$ mM) as a function of $[Mg^{2+}]$, for the simulations and for Schoppa et al.'s experimental results. The total charge decreases exponentially as a function of $[Mg^{2+}]$. The model is more sensitive to small Mg^{2+} concentrations than is the experimental preparation.

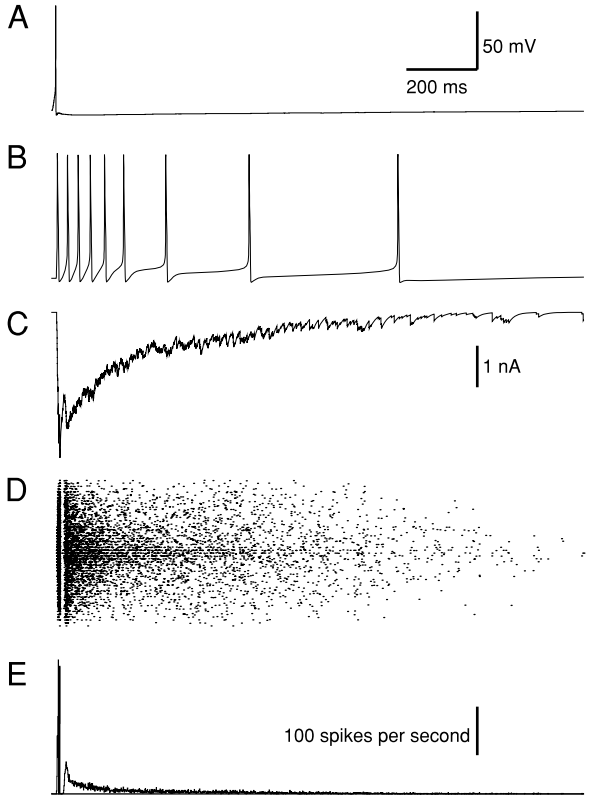

FIG. 2. Glomerular stimulation produces a single spike in all mitral cells (*A*), and prolonged firing in some granule cells (*B*). Overall granule cell response is a brief, synchronized burst, seen in the raster plot (*D*) and post-stimulus spike histogram (*E*), followed by unsynchronized firing that decays exponentially (*E*). The granule cells produce a prolonged inhibitory postsynaptic current (IPSC) in mitral cells (*C*), which is similar to that seen experimentally (Schoppa et al. 1998, their Fig. 1*A*), although the decay is faster. In the raster plot, each dot represents a spike and each row of dots is a different cell. The 2-dimensional structure of the network cannot be represented in this plot: the network is laid out row by row into a 1-dimensional array. Therefore neighboring lines in the plot do not necessarily represent neighboring cells in the array. Parameters: $n_{gran}/n_{mit} = 100$; $n_{syn} = 200$; $[Mg^{2+}] = 0$ mM.

Contributions of AMPA and NMDA receptors

To separate the contributions of the AMPA and NMDA receptors to the network response, the model was simulated with the conductances for these synapses set in turn to zero. The results are shown in Fig. 4. It is apparent that the NMDA receptor is needed to generate prolonged spike trains in the granule cell population (Fig. 4*B*) and hence to generate prolonged IPSCs in the mitral cells (Fig. 4*C*). The main effect of removing the AMPA current is to increase the rise time of the mitral cell IPSC. A second effect is to increase the amplitude of the prolonged granule cell population response: the peak of the baseline spike time histogram is 66 spikes/s while the peak of the non-AMPA histogram is 72 spikes/s (Fig. 4*D*). The mechanism for this may be that the double spike produced by the AMPA current causes a long refractory period, reducing the excitability of the granule cell population during the prolonged response.

Influence of network connectivity

The easily characterized response to glomerular shock provides a good opportunity to examine the effects of changing network connectivity parameters. The number of mitral cells, n_{mit}, was fixed throughout at 25. The number of granule cells, n_{gran}, was first fixed at 2,500 while the number of synapses per mitral cell, n_{syn}, was set at 50, 200, or 500. The results are shown in Fig. 5. Increasing n_{syn} increases the mean number of synapses per granule cell (0.5, 2.0, and 5.0 for the 3 cases), leading to faster and more prolonged granule cell firing in a larger number of cells. In turn, this decreases the rate of decay of the mitral cell IPSC. Increasing n_{syn} also increases the amplitude of the mitral cell IPSC. Decreasing n_{gran} has a similar effect to increasing n_{syn} (data not shown). When both n_{syn} and n_{gran} are increased together so as to keep the average number of synapses per granule cell constant, the effect dis-

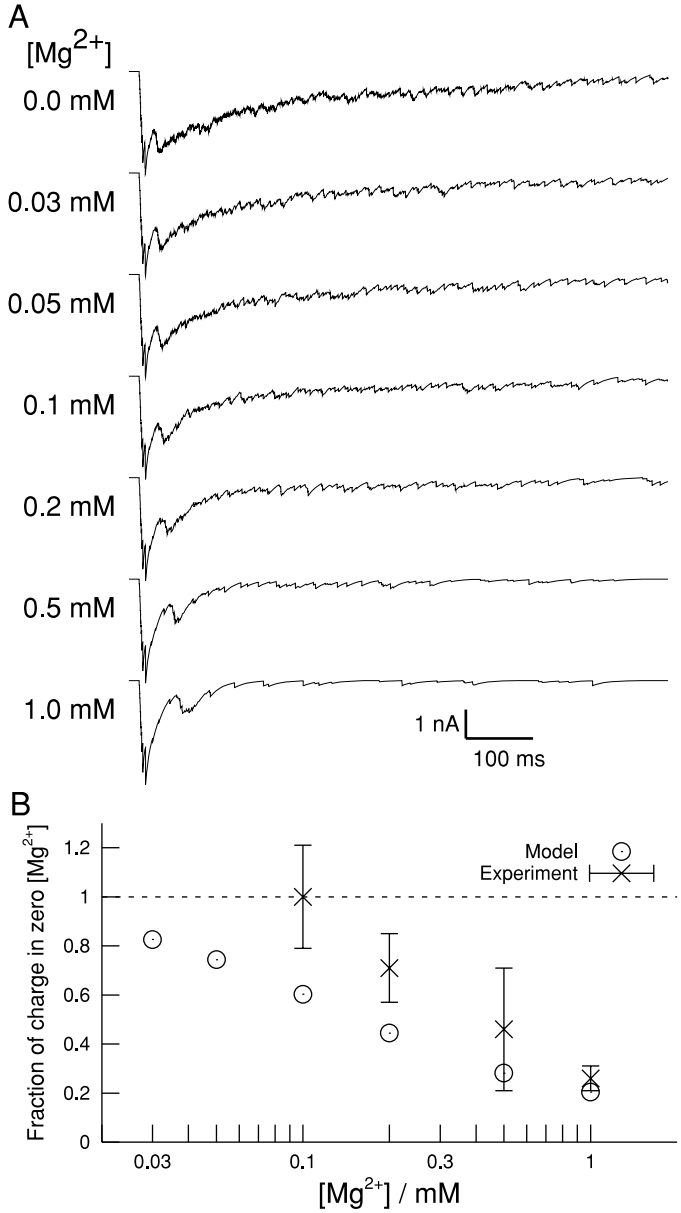

FIG. 3. *A*: increasing the external magnesium ion concentration, $[Mg^{2+}]$, reduces the duration of the mitral cell IPSC while having little effect on the peak current. *B*: total charge transferred to the cell (found by integrating the IPSC curve) is reduced exponentially by increasing $[Mg^{2+}]$. The sensitivity of the model (○) to $[Mg^{2+}]$ is greater than is found experimentally (Schoppa et al. 1998) (×).

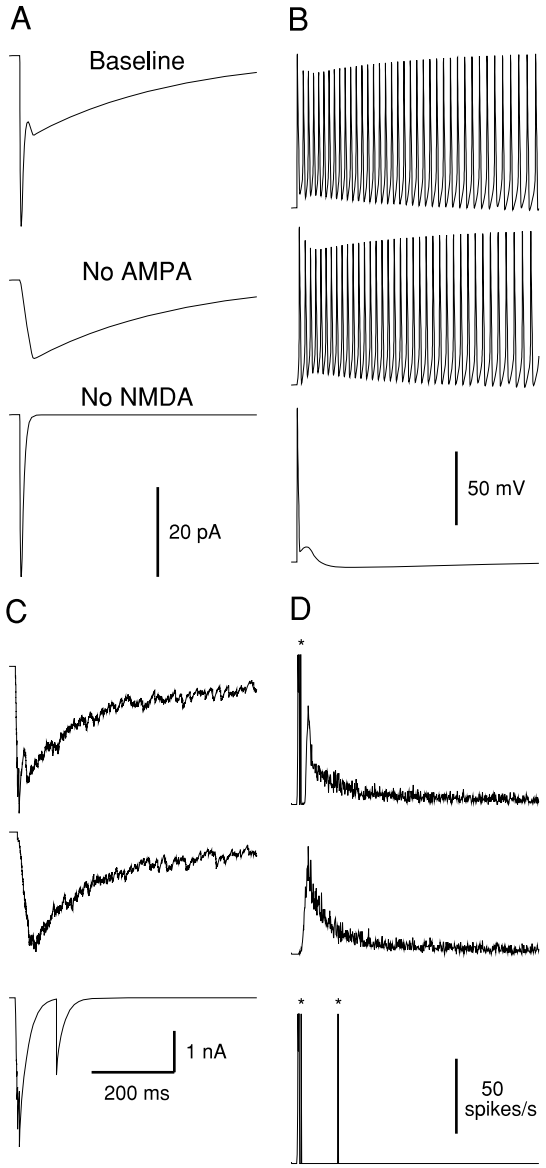

FIG. 4. The separate contributions of fast AMPA and slow *N*-methyl-D-aspartate (NMDA) currents to the granule cell excitatory postsynaptic current (EPSC) (*A*) in response to glomerular stimulation are clearly seen. While the presence of NMDA receptors alone is sufficient to produce a prolonged train of action potentials in granule cells (*B* and *D*), AMPA receptors alone produce only 1 or 2 spikes per cell, leading to a greatly-reduced duration of the IPSC in the mitral cells (*C*). Note that removing AMPA receptors increases the amplitude of the broad peak in the granule cell population spike-time histogram (STH) (*D*) compared with baseline. *D*: *bin has been truncated at 100 spikes.

appears—there is almost no change in the decay constant of the IPSC (data not shown). In summary, increasing the number of synapses onto granule cells increases the duration of the mitral cell IPSC.

We propose a simple mechanism for this effect (Fig. 6). We suppose that there is a threshold for the granule cell EPSC, below which the EPSC does not cause GABA release at the synapses onto mitral cells. Above this threshold, transmitter release is proportional to the height above the threshold. It does not matter whether the EPSP triggers action potentials, which lead to transmitter release, or whether the EPSP can cause transmitter release directly. The mitral cell IPSC is then proportional to the amount of transmitter released from the granule cell. A larger EPSC due to the activation of more synapses (Fig. 6, *right column*) will be above the threshold for a longer time than a smaller EPSC (Fig. 6, *left column*) and therefore the duration of the IPSC will be longer. By normalizing the IPSCs (Fig. 6, *bottom*) it is clear that the larger IPSC also has a slower decay rate and a faster onset.

Increasing the conductance of individual synapses, for example, through synaptic plasticity, or activating more of the existing synapses by stimulating more mitral cells should have the same effect as adding synapses.

Effect of granule–granule connections

Adding fast inhibitory synapses between granule cells, as described in METHODS, causes a small reduction in the early phase of the response (Fig. 7).

Response to odor stimulation

Having verified that the model gives a reasonable response to short-duration electrical stimulation, we proceeded to stimulate the bulb network model with an "odor-like" input. Except where noted, the network size was 6×6 mitral cells and 72×72 granule cells, and the number of synapses per mitral cell, n_{syn}, was 500. The range of synaptic connections was 0.5 times the size of the granule cell array ($r/r_{max} = 0.5$). The external

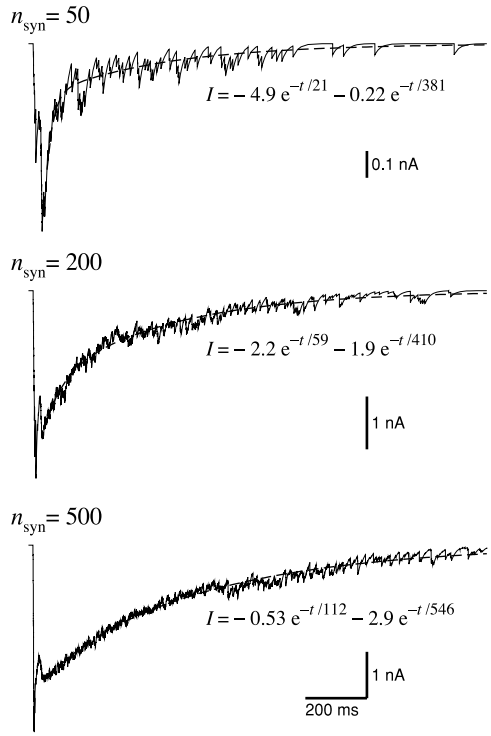

FIG. 5. Effect on the response to glomerular stimulation of changing the number of synapses per mitral cell (n_{syn}): increasing n_{syn} increases the average number of synapses per granule cell, leading to faster and more prolonged mitral cell firing. This in turn leads to slower decay of the mitral cell IPSC. Shown are the mitral cell IPSCs fitted with the sum of 2 exponentials. Increasing the number of synapses increases both time constants and increases the weight of the slow-time-constant term relative to the fast-time-constant term. *Bottom*: $GABA_A$ reversal potential was changed from 0 to −40 mV to prevent space clamp breakdown ($n_{syn} = 500$). This explains why the amplitude of the IPSC does not increase from the $n_{syn} = 200$ case.

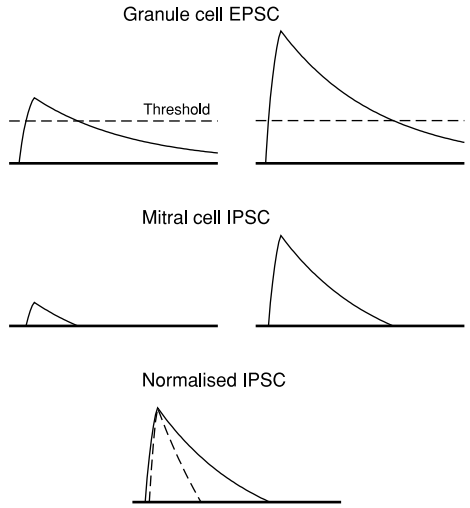

FIG. 6. Proposed mechanism for increased synaptic activation leading to slower reciprocal IPSCs. The amount of GABA released from granule cells is proportional to the height of the EPSC above some threshold (*top*). The size of the IPSC in the mitral cell (*middle*) is proportional to the amount of GABA released, and therefore a smaller EPSC (*left*) produces an IPSC that is both smaller and shorter than that produced by a larger EPSC (*right*). By normalizing the IPSCs (*bottom*), we can see that the smaller IPSC (dashed line) also decays faster than the larger IPSC (solid line).

magnesium ion concentration, $[Mg^{2+}]$, was set to 1 mM. The specific details of each experiment are given in the relevant section of RESULTS.

The response of the network model to a simulated odor stimulus that activates most glomeruli is shown in Fig. 8. For the first 1,000 ms, the mitral cells received weak "background" stimulation that did not cause those mitral cells that are activated to synchronize their firing, although there is some evidence of synchronization in the granule cell raster plot (Fig. 8*C*), which is not surprising due to the large "fan-out" from mitral to granule cells. Once the odor stimulus is added, both mitral and granule cells rapidly synchronize their firing. (We use the term synchronization in an approximate sense, since slower-firing cells tend to fire with a small phase-lag relative to the faster-firing cells.) Due to the synchronization of firing, mitral cell firing rates appear to be quantized, with most cells firing at the population response oscillation frequency of about 15 Hz or at some rational fraction of the population frequency. Because of this, the variability in output firing rates is less than the variability in input currents. However, the differences in output between neighboring cells can be much greater than the differences in input. The fastest-firing granule cells fire at the same rate as the fastest mitral cells but the majority of granule cells fire at lower rates.

It is possible that a critical mass of glomeruli must be activated to obtain synchronization. Therefore we simulated the same network with an odor that activated fewer than one-half of the glomeruli. With this stimulus, the mitral cells

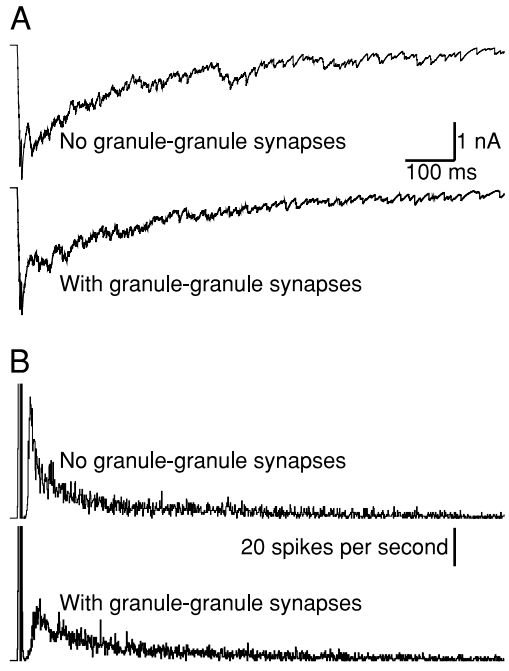

FIG. 7. Effect of granule–granule cell connections on the dendrodendritic inhibitory postsynaptic potential (IPSP). Granule–granule cell inhibition appears to affect principally the fastest-firing granule cells, reducing the initial rise in granule cell population activity (shown in STHs; *B*), and hence reducing the amplitude of the IPSC in mitral cells (*A*).

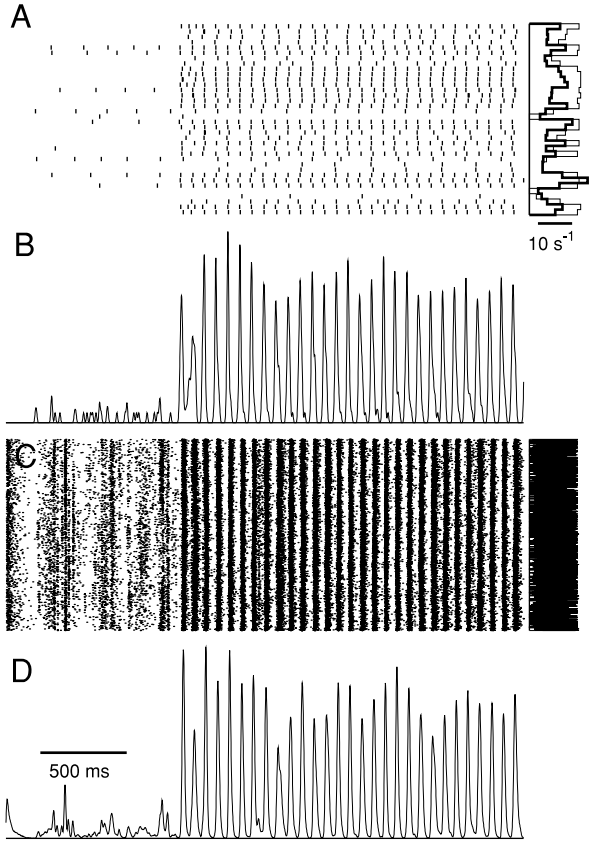

FIG. 8. Response of the mitral–granule network to a simulated odor stimulus. *A*: mitral cell raster plot and bar graph showing input currents (thick line) and output firing rates (thin line). *B*: mitral cell population smoothed STH (SSTH). The histogram was generated by summing Gaussian curves of area 1 centered on each spike time of each cell. This has the advantage over a normal histogram of not imposing arbitrary bins. The variance of the Gaussian functions was set to one-quarter of the mean inter-spike interval of the fastest firing cell. *C*: granule cell raster plot and bar graph showing output firing rates. *D*: granule cell population smoothed STH. Initially the network received weak, "background" stimulation. At 1,000 ms, the strong odor stimulus is added. The odor is one that activates most glomeruli. Both mitral and granule cells rapidly synchronize their firing at a rate of about 15 Hz. Parameters: $n_{mit} = 36$, $n_{gran}/n_{mit} = 144$, $r/r_{max} = 0.5$, $n_{syn} = 500$, odor intensity (I_{peak}) = 1.5 nA.

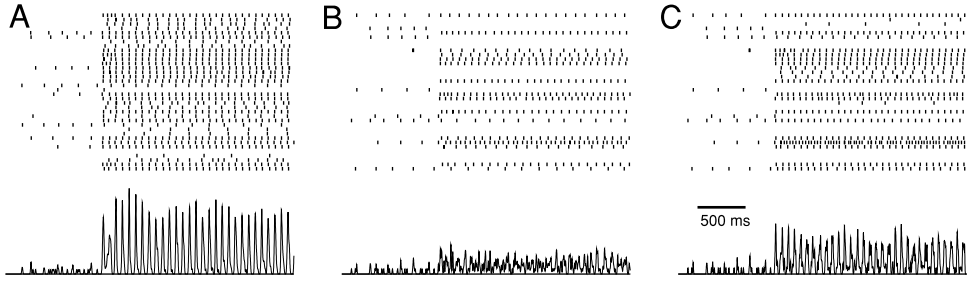

FIG. 9. Odors that stimulate more glomeruli more easily synchronize the mitral cell population. *A*: response to the same odor as in Fig. 8; (*top*) mitral cell raster plot; (*bottom*) mitral cell population SSTH. *B*: response to an odor that activates fewer glomeruli; same stimulus intensity as in *A*. *C*: response to the same odor as in *B*, but with the same total input current as in *A*. Parameters as for Fig. 8, except for *C*, odor intensity = 2.97 nA.

did not synchronize their firing globally (Fig. 9B), although there is some evidence for local synchronization between nearby pairs of cells. To test whether the loss of synchrony was merely due to the reduced total input to the network, we repeated the simulation with a higher odor intensity such that the total input current was the same as for the original odor (Fig. 9*C*). In this case, a few more glomeruli were recruited, although still fewer than with the original odor, and synchrony was recovered.

Effect of odor intensity

We investigated the effect of odor intensity on both the spatial activity pattern and the synchronization of the network by stimulating the model with the same odor input at different intensities, i.e., the input currents to different mitral cells were in the same ratio but the absolute magnitudes of the currents were changed. As a control, we also simulated a version of the model with no connections between mitral cells ($n_{syn} = 0$). The results are shown in Fig. 10. As the global input intensity is raised, for the same "odor" at different "concentrations," the number of activated mitral cells is increased, and the firing rate of activated mitral cells is increased, although this saturates at high-input levels. This saturation produces changes in the spatial activity pattern. Compared with the no-connections case, firing rates are lower with mitral–granule connections, and the responses saturate at lower levels. Synchronization of the responses is apparent for input levels of 0.9–1.0 nA and greater. Note that the synchronization index for the unconnected network is independent of the input current and hence of the firing rate. We repeated the simulations with different seeds for the random number generator (and hence difference connection patterns) at input levels of 0.8 and 1.2 nA. At 0.8 nA, there was no significant difference between the synchronization indices for the unconnected and connected models (*t*-test, $P = 0.06$, $n = 6$). At 1.2 nA, however, the difference was highly significant ($P = 3 \times 10^{-5}$, $n = 3$).

Contributions of AMPA and NMDA receptors

We showed earlier (see Fig. 4) that blocking AMPA receptors blocks the fast component of the reciprocal IPSP in mitral cells, whereas blocking NMDA receptors blocks the slow component. To determine the relative importance of AMPA and NMDA receptors to the network response to an odor stimulus we ran simulations *1*) under control conditions (cf. Fig. 8), *2*) without NMDA receptors in the granule cells, and *3*) without AMPA receptors (Fig. 11). Removing NMDA receptors had very little effect on the network response (Fig. 11*B*). In contrast, removing AMPA receptors had a significant effect: with a normal magnesium concentration ($[Mg^{2+}] = 1$ mM) the granule cells did not fire at all, and therefore the mitral cells were not synchronized (data not shown); in zero magnesium, the mitral cell network again synchronized its firing, but with

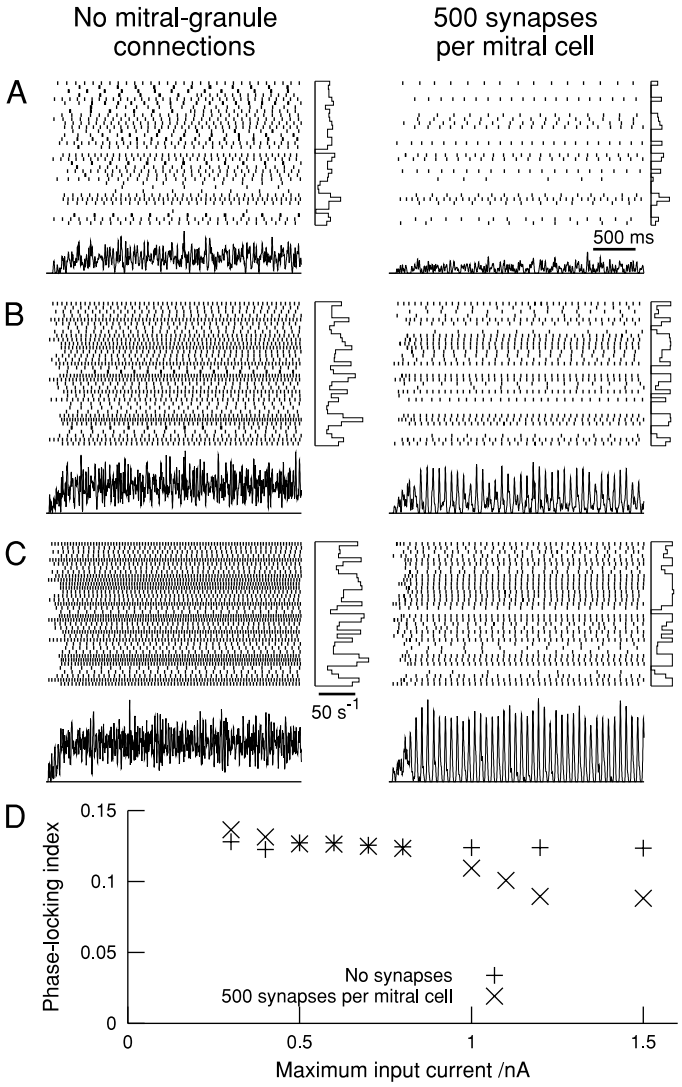

FIG. 10. Degree of synchronization increases as the odor intensity is increased. Each section of the figure shows the mitral cell raster plot, below which is an SSTH for mitral cell population and to the right of which is a bar graph showing the mean firing rate. *Left column*: control results for a network with no connections between mitral and granule cells and therefore no synchronization. *Right column*: results with 500 synapses per mitral cell. Maximum input current I_{peak} is (*A*) 0.5, (*B*) 1.0, and (*C*) 1.5 nA. *D*: phase-locking index as a function of the maximum input current for the control (+) and $n_{syn} = 500$ (×) cases. The phase-locking index differs significantly from the control case for $I_{peak} \geq 1.0$ nA. Parameters: $n_{mit} = 36$, $n_{gran}/n_{mit} = 144$, $r/r_{max} = 0.5$, $n_{syn} = 500$.

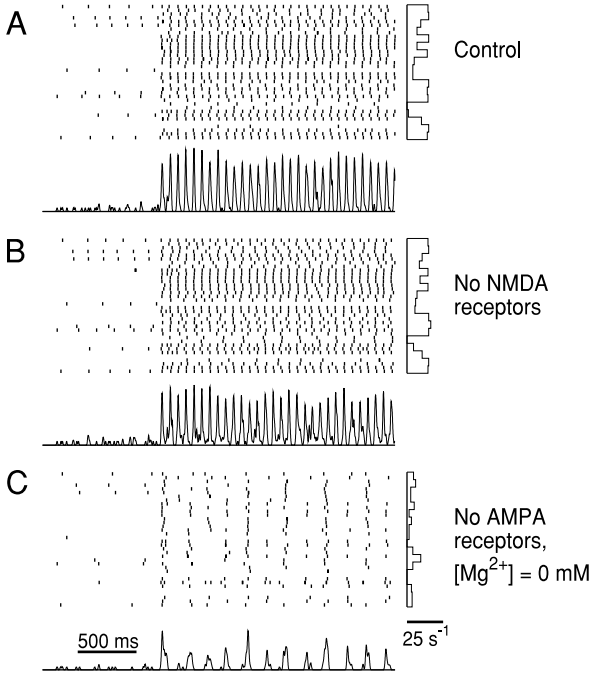

FIG. 11. Effect of AMPA and NMDA receptors on odor response. Each section of the figure shows the mitral cell raster plot, below which is an SSTH for the mitral cell population, and to the right of which is a bar graph showing the mean firing rate. *A*: under control conditions, the network synchronizes readily at a rate of about 15 Hz. *B*: removing NMDA receptors from granule cells has little effect on the response. Degree of synchronization is slightly less. *C*: with AMPA receptors removed and with $[Mg^{2+}] = 0$ mM to remove the NMDA receptor magnesium block, the network still synchronizes, but with a much lower firing rate of about 6 Hz. Parameters: $n_{mit} = 36$, $n_{gran}/n_{mit} = 144$, $r/r_{max} = 0.5$, $n_{syn} = 500$, $I_{peak} = 1.5$ nA.

a much lower firing rate (approximately 6 Hz) than the control (approximately 15 Hz; Fig. 11*C*). Therefore with physiological levels of magnesium, AMPA receptors, but not NMDA receptors, are required for synchronization in the model network. This is in contrast to what we might expect to find experimentally and points up an important limitation of the model: reciprocal inhibition is not dependent on NMDA receptor activation (see Fig. 4), although such activation greatly increases the duration of the IPSC, since the development of the granule cell model (Bhalla and Bower 1993) predates the experimental finding that reciprocal inhibition is entirely dependent on NMDA receptor activation (Isaacson and Strowbridge 1998; Schoppa et al. 1998). We would therefore expect that experimentally, and in contrast to the behavior of the current model, synchronization should be abolished by blocking NMDA receptors. The finding that blocking AMPA receptors in magnesium-free conditions results in synchronization at a slower rate is not inconsistent with existing experimental data and it would be interesting to test this prediction.

Effect of granule–granule connections

Adding mutually inhibitory connections between the basal dendrites of granule cells has very little effect on the behavior of the network model (Fig. 12). The most notable effect is a slight increase in the synchronized firing rate: from 30 to 31 spikes in 2 s. This is presumably because the increased inhibition of granule cells causes a reduction of inhibition of mitral cells, which therefore fire faster. The lack of effect of granule–

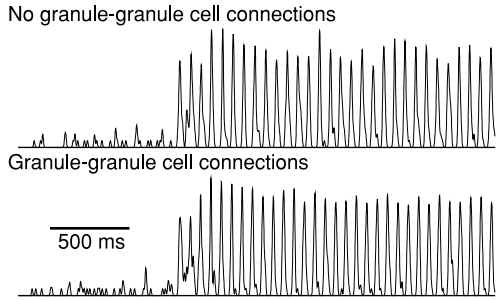

FIG. 12. Mitral cell SSTHs for a network with no granule–granule connections (*top*) and a network with granule–granule connections (*bottom*). Parameters: $n_{mit} = 36$, $n_{gran}/n_{mit} = 144$, $r/r_{max} = 0.5$, $n_{syn} = 500$, $I_{peak} = 1.5$ nA. Other parameters given in METHODS.

granule cell connections seems to be due to the location of the synapses—IPSPs in the passive basal dendrites have little effect on action potential initiation in the peripheral dendrites—and is in contrast to the important functional role the equivalent connections have in a model of the insect antennal lobe (Bazhenov et al. 2001b). It should be noted, however, that in the latter model the cells each comprise a single compartment, and so spatial effects cannot be seen.

Effect of varying the ratio of granule:mitral cells

As the size of the network is changed, so are the network properties. Since it is not possible to simulate a full-sized network, we were interested in whether simulating networks of different sizes would reveal some trend that would allow extrapolation of results to large networks. Therefore we changed the number of granule cells in the network while adjusting n_{syn} and $\bar{g}_{GABA_A}$ to keep the total input to granule and mitral cells approximately constant

$$\text{synapses per granule cell (mean)} = \frac{n_{mit}}{n_{gran}} n_{syn} = 3.472 \quad (3)$$

$$\text{peak mitral cell inhibition} = n_{syn}\bar{g}_{GABA_A} = 0.3\ \mu S \quad (4)$$

(see Table 2 for the parameter sets used). The changes in firing rate and phase-locking index of the mitral cells due to changing the number of granule cells were small, and there was no linear trend (Fig. 13).

Periodic stimulation

In natural situations, olfactory input to the mammalian olfactory bulb is periodic (due to breathing or sniffing), not constant. We investigated the response of the network to sine-wave current input, and found that at low frequency (0.5 Hz),

TABLE 2. *Parameters used to assess the effect of the number of granule cells on network synchronization*

n_{gran}/n_{mit}	n_{syn}	$\bar{g}_{GABA_A}$/nS
4	14	21.6
9	31	9.60
25	87	3.46
49	170	1.76
100	347	0.864
144	500	0.600
169	587	0.511

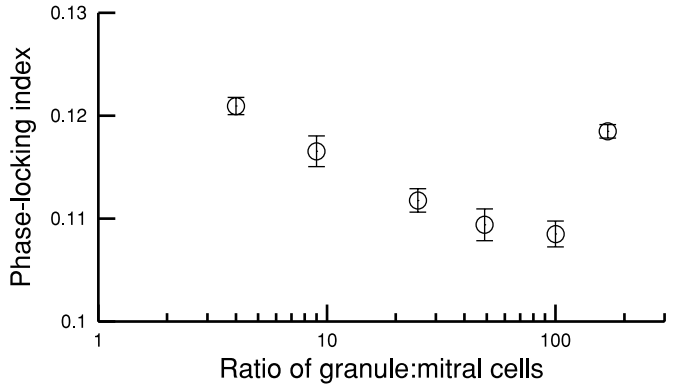

FIG. 13. Effect on synchronization of changing the ratio of granule:mitral cells. Each point shows the mean phase-locking index from 6 runs with different seeds for the random number generator (and hence different random connection patterns). Error bars show SE. Parameters: $n_{mit} = 36$, $r/r_{max} = 0.5$, $I_{peak} = 1.0$ nA.

the mitral cell population synchronizes its firing (seen as large, narrow peaks in the population spike time histogram; Fig. 14*A*). Increasing the amplitude of the stimulus reduces the latency to the onset of synchronization (data not shown).

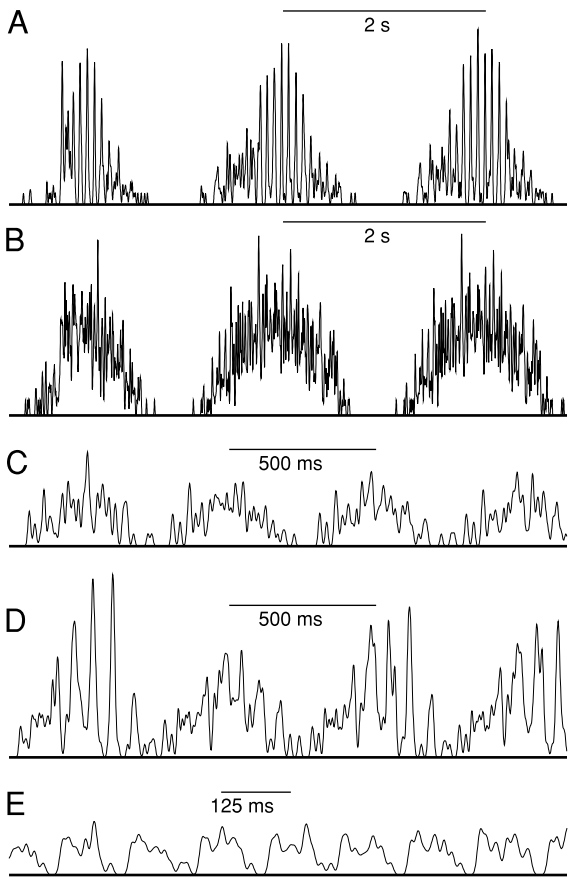

FIG. 14. Mitral cell STHs in response to periodic stimulation. All histograms have the same vertical scale. *A*: with 0.5-Hz stimulation, mitral cell synchronization (indicated by large "spikes" in the histogram) develops during each period of the input oscillation. *B*: as a control, with no dendrodendritic synapses, synchronization is not seen. *C*: with 2-Hz stimulation, synchronization does not develop. *D*: however, if the amplitude of the stimulus is increased (to 2.0 from 1.2 nA), synchronization of the mitral cell population does occur. *E*: at 8 Hz, it is not possible to synchronize the mitral cells. Parameters: $n_{mit} = 36$, $n_{gran}/n_{mit} = 144$, $r/r_{max} = 0.5$, $n_{syn} = 500$, odor intensity (I_{peak}) = 1.2 nA.

Increasing the stimulus frequency to 2 Hz eliminates synchronization (Fig. 14*C*), although it can be "rescued" by increasing the stimulus amplitude (Fig. 14*D*). With 8-Hz stimulation, which is within the range of sniffing frequencies in rats (although rapid fluctuations in air flow in the nasal cavity will not necessarily lead to rapid fluctuations in the input to the bulb due to the filtering effects of the molecular adsorption and transduction processes), synchronization of the mitral cells cannot be achieved (Fig. 14*E*).

Lateral inhibition

To determine whether the connections between mitral and granule cells give rise to lateral inhibition, we strongly stimulated a single mitral cell in a 10 × 10 array of uniformly weakly stimulated cells. The range of mitral–granule cell connections was set to 0.2 times the linear dimension of the granule cell array. To decrease simulation time we reduced the ratio of granule:mitral cells to 25, while compensating for this change by altering the number of mitral cell synapses and the $GABA_A$ conductance according to *Eqs. 3* and *4*.

Prior to stimulus onset, all cells fired with rates in the range of 5.2–6.1 Hz (Fig. 15*A*). For the duration of the stimulus presentation (2 s), the firing rate of the activated cell was 31 Hz. The firing rates of the nearest neighbors of the activated cell were depressed by about 1.5 Hz relative to the bulk of the mitral cell population (Fig. 15*B*). The experiment was repeated with a block of nine strongly activated cells (Fig. 15, *C* and *D*). The cells neighboring this block were more strongly suppressed than when a single mitral cell was activated strongly.

In this experiment, lateral inhibition could be seen clearly because the background activity was highly uniform across the mitral cell array. We next asked whether lateral inhibition could be seen with a more realistic, nonuniform distribution of

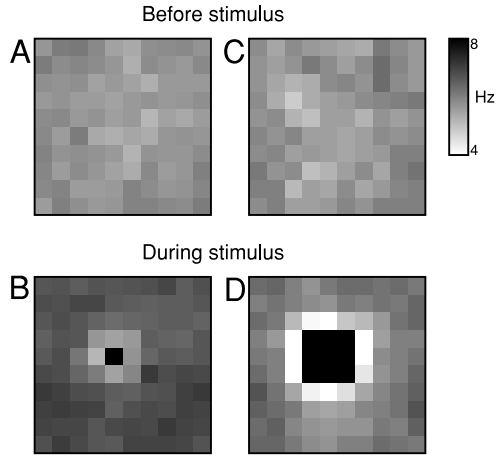

FIG. 15. Lateral inhibition in a 10 × 10 array of mitral cells with uniform background activity. Gray-scale value of each square represents the mean firing rate, averaged over 2 s of simulation. Firing rates above 8 Hz are represented by black. Firing rates below 4 Hz are represented by white. *A* and *C*: background firing rate, before stimulus onset. All cells receive the same input current. Differences in firing rate between them are due solely to random differences in connectivity. Range of firing rates is 5.2–6.1 Hz. *B*: stimulation of a single mitral cell, which fires at 31 Hz. Firing rates of neighboring cells are depressed by about 1.5 Hz relative to the bulk of the mitral cell population. *D*: stimulation of a 3 × 3 block of mitral cells, which fire at between 29 and 31 Hz. Firing rates of cells neighboring this block are depressed by about 3 Hz relative to the bulk of the population. Parameters: $n_{mit} = 100$, $n_{gran}/n_{mit} = 25$, $r/r_{max} = 0.2$, $n_{syn} = 86$, $\bar{g}_{GABA_A} = 3.46$ nA, $I_{peak} = 2.0$ nA.

background activity. In Fig. 16, unlike in Fig. 15, lateral inhibition is not obvious from comparing the before- (Fig. 16*A*) and during-stimulation (Fig. 16*B*) firing rate patterns. However, if we take the difference between these patterns to show the change in firing rate during stimulation (Fig. 16, *C* and *D*), it is clear that the nearest neighbors of strongly activated cells fire less rapidly during the stimulus.

Stimulation with two similar odors

One possible function of the olfactory bulb is to amplify the difference between the signals produced by similar odors. The responses of the bulb network model to two very similar odor stimuli are shown in Fig. 17. The input currents to the 64 cells of the network are shown in Fig. 17*A1*. The output mean firing rates, shown in Fig. 17*A2*, are mostly very similar for the two odors. However, a small number of cells with less-than-maximal firing rates show notable differences in the response to the two odors, e.g., cell 17 fires at a rate about one-half the maximum for Odor B but is silent for Odor A, while cell 45 fires for Odor A but is silent for Odor B. The olfactory cortex could use these significant differences in the responses of a small number of cells to discriminate between the odors. Looking at the temporal pattern of the response rather than just the mean firing rate reveals more obvious, global differences between the responses. This is clearly seen by comparing the population-averaged spike-time histograms in Fig. 17, *B* and *C*. In Fig. 17*C*, there is a waxing and waning pattern of synchronization, whereas in Fig. 17*B*, synchronization is late in developing but is then maintained for the duration of the recording. For very similar odorants, these differences may be a more robust way to discriminate between the odorants than the time-averaged firing rates.

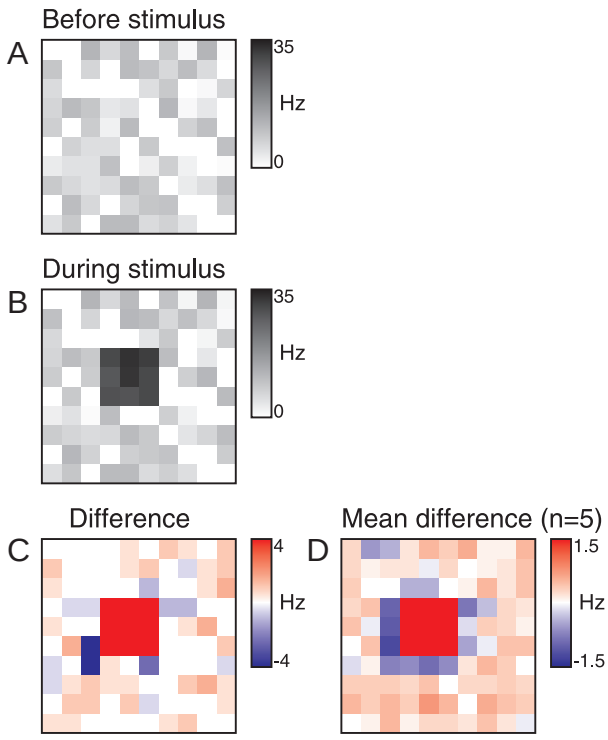

FIG. 16. Lateral inhibition in a 10 × 10 array of mitral cells with nonuniform background activity. *A*: background firing rate, before stimulus onset. Firing rates are in the range 0–12 Hz. *B*: stimulation of a 3 × 3 block of mitral cells, which fire with rates between 28 and 33 Hz. Because the background is nonuniform, it is impossible to see the depression of neighboring cells, unlike in Fig. 15*D*. *C*: change in firing rates when the stimulus is applied. Shades of red represent increases in firing rate, shades of blue represent decreases in firing rate. The color scales are clipped at 4 Hz (i.e., changes >4 Hz are represented by the same shade as changes equal to 4 Hz.) Decreases in firing rate are largest for some of the cells neighboring the stimulated block. This effect is clearer in *D*, which shows the firing rate change averaged over 5 runs of the model with different seeds for the random number generator. Parameters: $n_{mit} = 100$, $n_{gran}/n_{mit} = 25$, $r/r_{max} = 0.2$, $n_{syn} = 86$, $\bar{g}_{GABA_A} = 3.46$ nA, $I_{peak} = 2.0$ nA.

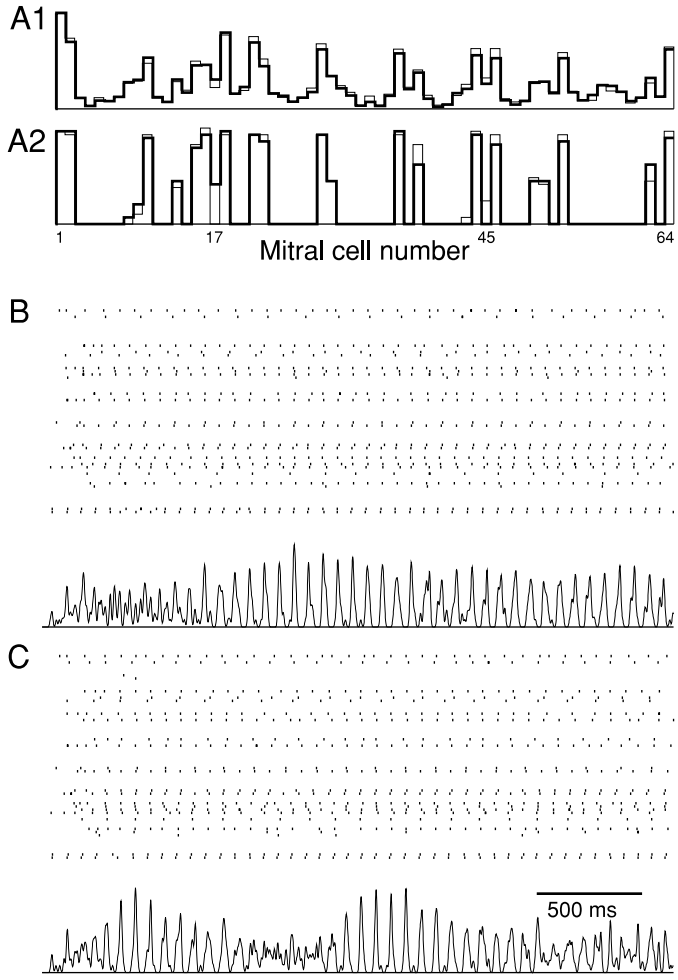

FIG. 17. Responses of the network model to stimulation with 2 similar odorants. *A1*: bar graph shows the relative strength of input to each of 64 mitral cells. Thick line, Odor A; thin line, Odor B. Note that the mitral cells are arranged in an 8 × 8 array. *A2*: output firing rates of the cells, averaged over a 2-s interval. Differences in the cell outputs are mostly small, except for a small number of cells for which there is a large difference in firing rate. *B* and *C*: granule cell raster plots and SSTHs for stimulation with (*B*) Odor A and (*C*) Odor B. Slow temporal changes in the power of the global oscillation are quite different in the 2 cases: slow onset of synchronization followed by a constant level of synchronization for Odor A, and rapid onset followed by waxing and waning of synchronization for Odor B. Parameters: $n_{mit} = 64$, $n_{gran}/n_{mit} = 49$, $r/r_{max} = 0.25$, $n_{syn} = 500$, $I_{peak} = 1.0$ nA.

DISCUSSION

We have developed a detailed, realistic model of the mitral–granule cell circuits in the olfactory bulb that we have used to investigate the spatio-temporal processing of odor information. The results confirm our hypothesis that lateral inhibition and

network synchronization will arise naturally from a model consisting only of mitral and granule cells, with parameters obtained from the literature and not from tuning the model, although there are many discrepancies between model and data that can be resolved by further modeling efforts.

Dendrodendritic inhibition

The model was tested by attempting to reproduce published data on dendrodendritic synaptic currents (Schoppa et al. 1998). The simulated mitral cell IPSC matched the experimental one closely when the number of synapses per mitral cell was a few hundred. Since we estimate that a real mitral cell makes on the order of 10^4 synapses with granule cells, we predict that real reciprocal synapses are less effective than in our model. Possible reasons for this are *1*) synaptic failure, the probability of vesicle release due to a presynaptic action potential is likely to be less than one; and *2*) granule cells may be less responsive than in our model (see Validity and limitations of the model).

A new finding from our simulation results is that the time course as well as the amplitude of reciprocal and lateral inhibition is affected by the degree of granule cell activation. Increasing the effective number of synapses per granule cell increases the time constant of the mitral cell IPSC. The time constant may be longer than that of the NMDA current that underlies the granule cell response; this was observed experimentally by Schoppa et al. (1998), and our finding suggests a possible mechanism for this prolongation, although other mechanisms, such as second-messenger signaling in the granule cell or recurrent self-excitation of the mitral cell dendrite, are possible. It may be possible to see this effect directly in a slice preparation by using low concentrations of glutamate channel blockers to reduce but not eliminate granule cell excitation by mitral cells. We would expect that the IPSC duration would decrease as the concentration of glutamate blockers was increased. This effect leads to a number of predictions: *1*) stimulation of a single tufted cell should produce a shorter IPSC than stimulation of a single mitral cell, since the shorter dendrites of the tufted cell make fewer synapses and so are less effective in exciting the granule cell population; *2*) the duration of IPSCs in vivo should be longer than in the slice preparation, since in the slice many mitral cell secondary dendrites are cut short, and so make fewer synapses; and *3*) modulation of granule cell excitability by centrifugal inputs will affect the temporal structure of the bulb response and could promote or suppress synchronization. The first of these predictions is borne out by published data: the IPSC time constant measured in tufted cells (approximately 290 ms; Christie et al. 2001) is significantly shorter than for mitral cells (approximately 460 ms; Schoppa et al. 1998).

Response to odor stimuli

In response to simulated odor stimuli, the mitral cell population in the model readily synchronizes its action potential firing, despite randomness in the connections and variability in the drive to individual cells. Global synchronization is promoted by *1*) high-input intensity and *2*) long-range connections. Synchronization develops over a few hundred milliseconds; therefore constant or low-frequency stimulation is optimum and synchronization may not be important during rapid sniffing, although it should be noted that the model parameters are from experiments at room temperature; at higher temperatures the network kinetics are expected to be faster and synchronization may persist at higher stimulus frequencies.

What is the mechanism of synchronization? It has been shown in theoretical studies that networks of mutually inhibitory cells with all-to-all connectivity will phase-lock provided the variability of the drive to the cells is not too large (Chow 1998; Davison 2001). If we regard the mitral cells as being mutually inhibitory via the granule cells, then the olfactory bulb network matches the theoretical case. All-to-all connectivity is apparently not required for robust synchronization. In the control case, the synchronized firing frequency (approximately 15 Hz) is determined by the intrinsic mitral cell firing frequency and by the time constant of the $GABA_A$ receptor, since the amplitude of I_{GABA_A} between action potentials is much greater than the amplitudes of the membrane currents (data not shown). This frequency is rather lower than the 40–60 Hz gamma frequency oscillations seen in vivo. This discrepancy may possibly be explained by a limitation of the mitral cell model used in our network: the cell cannot fire faster than 40 Hz (Davison et al. 2000) and the synchronization frequency must be less than this. In addition, the measurement of the $GABA_A$ time constant was performed at room temperature. At body temperature, the $GABA_A$ receptor is likely to have faster kinetics, and therefore the synchronization frequency will be higher.

It has been suggested in insect olfactory systems that while the spatial, time-averaged response pattern is sufficient for discrimination between dissimilar odorants, distinguishing very similar odorants relies on synchronization between output neurons (Stopfer et al. 1997). Here we have shown by modeling that two stimuli that produce almost indistinguishable spatial activity patterns may cause very different temporal sequences of synchronization. We have measured only global synchrony, whereas local synchronization may be more useful in odor processing. Nevertheless, these results provide support for the hypothesis that the same principles apply in the mammalian olfactory bulb as in the insect antennal lobe.

The model has fewer cells than the real olfactory bulb and therefore has higher connectivity. High connectivity means that distant cells communicate easily and so synchronization is more likely to occur. We define the "connection fraction" (CF) as the percentage of the granule cells within its dendritic arbor to which a mitral cell is connected and the "mutual connection fraction" (MCF) as the percentage of the granule cells connected to one mitral cell that are also connected to any other given, neighboring, mitral cell. We have previously estimated these metrics for the rabbit olfactory bulb: CF approximately 4%, MCF approximately 4% (Davison 2001). For the model, CF = 12% and MCF approximately 15%. Therefore the connectivity of the real bulb is about one-third that of the model, and so synchronization will not be seen as readily. Experimentally, synchronization was seen in 27% of cell pairs recorded in the rabbit olfactory bulb in vivo (Kashiwadani et al. 1999). Synchronization is less likely to be seen in the slice preparation, since much of the mitral cell secondary dendrite arbor is not preserved.

It has been hypothesized that lateral inhibition between M/T cells, mediated via granule cells, gives rise to a center-surround receptive field leading to a sharpening of the tuning specificity

of the cells (Mori et al. 1999; Yokoi et al. 1995). Given that the length of mitral cell secondary dendrites is much greater than the distance between adjacent glomeruli, however, it is unclear whether lateral inhibition is sufficiently spatially localized to produce a center-surround pattern. The results presented here (Figs. 15 and 16) suggest that it is: inhibition of neighboring cells/glomeruli extends only to the nearest neighbors in the 10×10 array while the range of connections is twice this. This is presumably because the greatest density of mutual connections occurs for neighboring cells. This result may be dependent on the effective lack of branching in our model "dendrites"; however, increased branching would raise the density of connections at larger distances from the soma. We also note that lateral inhibition is not uniform. With nonuniform background activity some of the neighboring neurons are strongly suppressed while others are unaffected.

Validity and limitations of the model

The cell models used here are morphologically simplified versions of the detailed models published by Bhalla and Bower (1993). For the mitral cell, subsequent experimental studies are broadly consistent with their model in terms of the presence and distribution of channels (e.g., for A-type potassium channels (Chen and Shepherd 1997; Wang et al. 1996) and L-type calcium channels (Bischofberger and Schild 1995; Schild et al. 1995). Exceptions are the experimental findings of subthreshold membrane potential oscillations (Desmaisons et al. 1999) and membrane potential bistability (Heyward et al. 2001). For a more complete discussion, see Davison (2001). The most significant limitation of the granule cell model is the lack of A-type potassium channels in the dendrites, since Schoppa and Westbrook (1999) measured the A-current to be much larger in comparison to the delayed rectifier current in the dendrites than in the soma. This is important because of the crucial role of the A-current in regulating mitral–granule synaptic communication (Isaacson and Strowbridge 1998; Schoppa and Westbrook 1999; Schoppa et al. 1998). This limitation, which increases the granule cell excitability in the model compared with the real bulb, is offset by another of the model's limitations, the reduced number of synapses in the model.

The morphologically simplified models used in the network fit the full Bhalla-Bower models closely in terms of action potential timing (Davison et al. 2000). In a network in which neurons communicate via spike-triggered synapses, these reduced models are therefore a valid substitute. However, they ignore most of the information processing that may be occurring within dendrites and spines (Chen et al. 1997; Xiong and Chen 2002). The mitral cell model separates primary and secondary dendrites, but interactions between synapses on the same dendrite cannot be represented. The current model should be considered a first approximation; morphologically detailed models will give a fuller picture.

Recent studies have shown that calcium entry through NMDA receptors and voltage-gated ion channels has an important role in the granule cell response to dendrodendritic excitation (Chen et al. 2000; Halabisky et al. 2000; Isaacson 2001). None of this detail is included in the current model, which again, should be considered a first approximation.

Our reasons for not including periglomerular cells in the model were given in METHODS. Nevertheless, PG cells must have an important role in the mammalian olfactory bulb, and adding them to the model is a high priority for future versions. The results presented here will serve as a baseline against which the effects of PG cells can be measured. Similarly, in this model, tufted cells are assumed to be equivalent to mitral cells or to be involved in a largely separate, functionally independent circuit. A full model should take account of the different properties of mitral and tufted cells.

Other olfactory bulb models

We are not aware of any existing olfactory bulb models with a level of detail and biological fidelity comparable to the model we present here. The model of White et al. (1992) is of a similar, although less detailed, nature. However, there are a number of simpler, more abstract models in the literature (e.g., Li 1990; Linster and Hasselmo 1997). The model of Linster and Hasselmo (1997) is based on known anatomy, with synaptic weights and transmission delays tuned by comparing model output to experimental field potentials and EEG (in contrast to the model described herein, for which these parameters were based on direct experimental measurements). The main conclusion of their work is that the bulb acts to make the odor representation more sparse: periglomerular cell activity affects the number of active mitral/tufted cells, while granule cell activity determines the response intensity of active mitral cells. Our model does not have PG cells, but we find that granule cells can play the role ascribed to PG cells in their model, reducing the number of active mitral cells.

There are several models of the antennal lobe, a structure in insects analogous to the olfactory bulb (Bazhenov et al. 2001a,b; Linster and Cleland 2001). The model of Bazhenov et al. (2001a,b) includes a similar level of detail to our model, although the cell models are all single-compartment.

CONCLUSIONS

We have developed the most detailed, realistic, and thoroughly investigated model of the mammalian olfactory bulb published to date. Future refinements and extensions of the model will include the incorporation of PG and tufted cells, updating the cell models, and modeling the dendrodendritic synapses in more detail, particularly the role of calcium in neurotransmitter release. There are many further questions about the bulb that can be addressed using the model: what are the different roles of the two levels of inhibition of mitral/tufted cells (by periglomerular cells in the glomeruli and by granule cells in the external plexiform layer)? How do the functions of mitral and tufted cells differ? How does synaptic plasticity affect information processing in the olfactory bulb? We believe that a synergy between experimental and theoretical approaches will allow us to make the most rapid progress in understanding the olfactory system.

APPENDIX

In this APPENDIX, we give a full description of the equations for the synaptic models. They are based on the models of Destexhe et al. (1998). The synaptic currents induced by a presynaptic spike at time t_0 are

$$I_{\mathrm{AMPA}}(V,t) = \bar{g}_{\mathrm{AMPA}} e^{-t'/\tau_{\mathrm{AMPA}}} (V(t) - E_{\mathrm{E}}) \qquad t' > 0 \tag{5}$$

$$I_{\mathrm{GABA_A}}(V,t) = \bar{g}_{\mathrm{GABA_A}} e^{-t'/\tau_{\mathrm{GABA_A}}}(V(t) - E_I) \qquad t' > 0 \tag{6}$$

$$I_{\mathrm{NMDA}}(V,t,[\mathrm{Mg}^{2+}]) = \bar{g}_{\mathrm{NMDA}} B(V,[\mathrm{Mg}^{2+}]) r(t')(V(t) - E_E) \qquad t' > 0 \tag{7}$$

$$r(t') = \begin{cases} (1 - e^{-t'/\tau^{\alpha}_{\mathrm{NMDA}}}) & 0 < t' \le t_{\mathrm{dur}} \\ r(t_{\mathrm{dur}}) e^{-(t'-t_{\mathrm{dur}})/\tau^{\beta}_{\mathrm{NMDA}}} & t' > t_{\mathrm{dur}} \end{cases} \tag{8}$$

where $V(t)$ is the membrane potential, $t' = t - t_0 - t_d$, t_d is the synaptic time decay ($t_d = t_I$ for the $GABA_A$ synapses, $t_d = t_E$ for the AMPA and NMDA synapses), $\bar{g}_{\mathrm{AMPA}}$, $\bar{g}_{\mathrm{GABA_A}}$, and $\bar{g}_{\mathrm{NMDA}}$ are the maximal conductances for the AMPA, $GABA_A$, and NMDA synapses, respectively, E_E and E_I are the reversal potentials for the excitatory and inhibitory synapses, respectively, τ_{AMPA} and $\tau_{\mathrm{GABA_A}}$ are the decay time constants for the AMPA and $GABA_A$ synapses, $\tau^{\alpha}_{\mathrm{NMDA}}$ is the time constant for the rising phase and $\tau^{\beta}_{\mathrm{NMDA}}$ is the time constant for the decaying phase of the NMDA conductance, t_{dur} is the duration of the NMDA rise phase, $[\mathrm{Mg}^{2+}]$ is the external magnesium concentration (in mM), and $B(V, [\mathrm{Mg}^{2+}])$ is the voltage-dependent magnesium block, given by

$$B(V,[\mathrm{Mg}^{2+}]) = \left(1 + \frac{e^{-0.062V}[\mathrm{Mg}^{2+}]}{3.57}\right) \tag{9}$$

The equation for the granule–granule cell $GABA_A$ synapse is the same as *Eq. 6*, but the values of the parameters are different (indicated with a superscript *g* in Table 1).

We thank Drs. W. Chen and T. Morse for helpful comments on the manuscript.

DISCLOSURES

This work was supported by the Biotechnology and Biological Sciences Research Council of Great Britain.

REFERENCES

Adrian ED. Olfactory reactions in the brain of the hedgehog. *J Physiol* 100: 459–473, 1942.

Bardoni R, Magherini PC, and Belluzzi O. Sodium current in periglomerular cells of frog olfactory bulb in vitro. *Brain Res* 703: 19–25, 1995.

Bardoni R, Puopolo M, Magherini PC, and Belluzzi O. Potassium currents in periglomerular cells of frog olfactory bulb in vitro. *Neurosci Lett* 210: 95–98, 1996.

Bazhenov M, Stopfer M, Rabinovich M, Abarbanel H, Sejnowski T, and Laurent G. Model of cellular and network mechanisms for odor-evoked temporal patterning in the locust antennal lobe. *Neuron* 30: 569–581, 2001a.

Bazhenov M, Stopfer M, Rabinovich M, Huerta R, Abarbanel H, Sejnowski T, and Laurent G. Model of transient oscillatory synchronization in the locust antennal lobe. *Neuron* 30: 553–567, 2001b.

Bhalla US and Bower JM. Exploring parameter space in detailed single cell models: simulations of the mitral and granule cells of the olfactory bulb. *J Neurophysiol* 69: 1948–1965, 1993.

Bischofberger J and Schild D. Different spatial patterns of $[Ca^{2+}]$ increase caused by N- and L-type Ca^{2+} channel activation in frog olfactory bulb neurones. *J Physiol* 487: 305–317, 1995.

Buonviso N, Chaput MA, and Scott JW. Mitral cell-to-glomerulus connectivity—an HRP study of the orientation of mitral cell apical dendrites. *J Comp Neurol* 307: 57–64, 1991.

Chen WR, Midtgaard J, and Shepherd GM. Forward and backward propagation of dendritic impulses and their synaptic control in mitral cells. *Science* 278: 463–467, 1997.

Chen WR and Shepherd GM. Membrane and synaptic properties of mitral cells in slices of rat olfactory bulb. *Brain Res* 745: 189–196, 1997.

Chen WR, Xiong W, and Shepherd GM. Analysis of relations between NMDA receptors and GABA release at olfactory bulb reciprocal synapses. *Neuron* 25: 625–633, 2000.

Chow CC. Phase-locking in weakly heterogeneous neuronal networks. *Physica D* 118: 343–370, 1998.

Christie JM, Schoppa NE, and Westbrook GL. Tufted cell dendrodendritic inhibition in the olfactory bulb is dependent on NMDA receptor activity. *J Neurophysiol* 85: 169–173, 2001.

Davison AP. *Mathematical modelling of information processing in the olfactory bulb* (PhD thesis). Cambridge, UK: Univ. of Cambridge, 2001.

Davison AP, Feng J, and Brown D. A reduced compartmental model of the mitral cell for use in network models of the olfactory bulb. *Brain Res Bull* 51: 393–399, 2000.

Desmaisons D, Vincent JD, and Lledo PM. Control of action potential timing by intrinsic subthreshold oscillations in olfactory bulb output neurons. *J Neurosci* 19: 10727–10737, 1999.

Destexhe A, Mainen ZF, and Sejnowski TJ. Kinetic models of synaptic transmission. In: *Methods in Neuronal Modeling: From Ions to Networks* (2nd ed.), edited by Koch C and Segev I. Cambridge, MA: MIT Press, 1998.

Didier A, Carleton A, Bjaalie JG, Vincent J-D, Ottersen OP, Storm-Mathisen J, and Lledo P-M. A dendrodendritic reciprocal synapse provides a recurrent excitatory connection in the olfactory bulb. *Proc Natl Acad Sci USA* 98: 6441–6446, 2001.

Dryer L and Graziadei PPC. Mitral cell dendrites—a comparative approach. *Anat Embryol (Berl)* 189: 91–106, 1994.

Ezeh PI, Wellis DP, and Scott JW. Organization of inhibition in the rat olfactory bulb external plexiform layer. *J Neurophysiol* 70: 263–274, 1993.

Halabisky B, Friedman D, Radojicic M, and Strowbridge BW. Calcium influx through NMDA receptors directly evokes GABA release in olfactory bulb granule cells. *J Neurosci* 20: 5124–5134, 2000.

Heyward P, Ennis M, Keller A, and Shipley MT. Membrane bistability in olfactory bulb mitral cells. *J Neurosci* 21: 5311–5320, 2001.

Hinds JW and McNelly NA. Aging of the rat olfactory bulb: growth and atrophy of constituent layers and changes in size and number of mitral cells. *J Comp Neurol* 171: 345–368, 1977.

Hines ML and Carnevale NT. The NEURON simulation environment. *Neural Comput* 9: 1179–1209, 1997.

Isaacson JS. Glutamate spillover mediates excitatory transmission in the rat olfactory bulb. *Neuron* 23: 377–384, 1999.

Isaacson JS. Mechanisms governing dendritic γ-aminobutyric acid (GABA) release in the rat olfactory bulb. *Proc Natl Acad Sci USA* 98: 337–342, 2001.

Isaacson JS and Strowbridge BW. Olfactory reciprocal synapses: dendritic signalling in the CNS. *Neuron* 20: 749–761, 1998.

Kashiwadani H, Sasaki YF, Uchida N, and Mori K. Synchronized oscillatory discharges of mitral/tufted cells with different molecular receptive ranges in the rabbit olfactory bulb. *J Neurophysiol* 82: 1786–1792, 1999.

Kishi K, Mori K, and Ojima H. Distribution of local axon collaterals of mitral, displaced mitral, and tufted cells in the rabbit olfactory-bulb. *J Comp Neurol* 225: 511–526, 1984.

Laurent G, Stopfer M, Friedrich RW, Rabinovich MI, Volkovskii A, and Abarbanel HDI. Odor encoding as an active, dynamical process: experiments, computation, and theory. *Annu Rev Neurosci* 24: 263–297, 2001.

Li Z. A model of olfactory adaptation and sensitivity enhancement in the olfactory bulb. *Biol Cybern* 62: 349–361, 1990.

Linster C and Cleland TA. How spike synchronization among olfactory neurons can contribute to sensory discrimination. *J Comput Neurosci* 10: 187–193, 2001.

Linster C and Hasselmo M. Modulation of inhibition in a model of olfactory bulb reduces overlap in the neural representation of olfactory stimuli. *Behav Brain Res* 84: 117–127, 1997.

Luo M and Katz LC. Response correlation maps of neurons in the mammalian olfactory bulb. *Neuron* 32: 1165–1179, 2001.

McQuiston AR and Katz L. Electrophysiology of interneurons in the glomerular layer of the rat olfactory bulb. *J Neurophysiol* 84: 1899–1907, 2001.

Mori K, Kishi K, and Ojima H. Distribution of dendrites of mitral, displaced mitral, tufted, and granule cells in the rabbit olfactory-bulb. *J Comp Neurol* 219: 339–355, 1983.

Mori K, Nagao H, and Yoshihara Y. The olfactory bulb: coding and processing of odor molecule information. *Science* 286: 711–715, 1999.

Mori K and Takagi SF. An intracellular study of dendrodendritic inhibitory synapses on mitral cells in the rabbit olfactory bulb. *J Physiol* 279: 569–588, 1978.

Nusser Z, Kay LM, Laurent G, Homanics GE, and Mody I. Disruption of $GABA_A$ receptors on GABAergic interneurons leads to increased oscillatory power in the olfactory bulb network. *J Neurophysiol* 86: 2823–2833, 2001.

Orona E, Rainer EC, and Scott JW. Dendritic and axonal organization of mitral and tufted cells in the rat olfactory-bulb. *J Comp Neurol* 226: 346–356, 1984.

Orona E, Scott JW, and Rainer EC. Different granule all populations innervate superficial and deep regions of the external plexiform layer in rat olfactory bulb. *J Comp Neurol* 217: 227–237, 1983.

Panhuber H, Laing DG, Willcox ME, Eagleson GK, and Pittman EA. The distribution of the size and number of mitral cells in the olfactory-bulb of the rat. *J Anat* 140: 297–308, 1985.

Price JL and Powell TPS. The synaptology of the granule cells of the olfactory bulb. *J Cell Sci* 7: 125–155, 1970.

Puopolo M and Belluzzi O. Sodium current in periglomerular cells of rat olfactory bulb in vitro. *Neuroreport* 7: 1846–1850, 1996.

Puopolo M and Belluzzi O. Functional heterogeneity of periglomerular cells in the rat olfactory bulb. *Eur J Neurosci* 10: 1073–1083, 1998.

Reyher CKH, Lübke J, Larsen WJ, Hendrix GM, Shipley MT, and Baumgarten HG. Olfactory bulb granule cell aggregates: morphological evidence for interperikaryal electrotonic coupling via gap junctions. *J Neurosci* 11: 1485–1495, 1991.

Royet JP, Distel H, Hudson R, and Gervais R. A re-estimation of the number of glomeruli and mitral cells in the olfactory bulb of rabbit. *Brain Res* 788: 35–42, 1998.

Schild D, Geiling H, and Bischofberger J. Imaging of L-type Ca^{2+} channels in olfactory bulb neurones using fluorescent dihydropyridine and a styryl dye. *J Neurosci Methods* 59: 183–190, 1995.

Schneider SP and Scott JW. Orthodromic response properties of rat olfactory bulb mitral and tufted cells correlate with their projection patterns. *J Neurophysiol* 50: 358–378, 1983.

Schoppa NE, Kinzie JM, Sahara Y, Segerson TP, and Westbrook GL. Dendrodendritic inhibition in the olfactory bulb is driven by NMDA receptors. *J Neurosci* 18: 6790–6802, 1998.

Schoppa NE and Westbrook GL. Regulation of synaptic timing in the olfactory bulb by an A-type potassium current. *Nature Neurosci* 2: 1106–1113, 1999.

Schoppa NE and Westbrook GL. Glomerulus-specific synchronization of mitral cells in the olfactory bulb. *Neuron* 31: 639–651, 2001.

Shepherd GM and Greer CA. Olfactory bulb. In: *The Synaptic Organization of the Brain* (4th ed.), edited by Shepherd GM. Oxford: Oxford, 1998, chapt. 5, p. 159–203.

Stopfer M, Bhagavan S, Smith BH, and Laurent G. Impaired odour discrimination on desynchronisation of odour-encoding neural assemblies. *Nature* 390: 70–74, 1997.

Wang XY, McKenzie JS, and Kemm RE. Whole-cell K^+ currents in identified olfactory bulb output neurones of rats. *J Physiol* 490: 63–77, 1996.

Wellis DP and Kauer JS. GABAergic and glutamatergic synaptic input to identified granule cells in salamander olfactory bulb. *J Physiol* 475: 419–430, 1994.

White J, Hamilton KA, Neff SR, and Kauer JS. Emergent properties of odor information coding in a representational model of the salamander olfactory bulb. *J Neurosci* 12: 1772–1780, 1992.

Xiong W and Chen WR. Dynamic gating of spike propagation in the mitral cell lateral dendrites. *Neuron* 34: 1–20, 2002.

Xu F, Greer CA, and Shepherd GM. Odor maps in the olfactory bulb. *J Comp Neurol* 422: 489–495, 2000.

Yokoi M, Mori K, and Nakanishi S. Refinement of odor molecule tuning by dendrodendritic synaptic inhibition in the olfactory bulb. *Proc Natl Acad Sci USA* 92: 3371–3375, 1995.